

# Crystal and Solution Structures of the Helicase-binding Domain of *Escherichia coli* Primase\*<sup>§</sup>

Received for publication, November 8, 2004, and in revised form, December 22, 2004  
Published, JBC Papers in Press, January 12, 2005, DOI 10.1074/jbc.M412645200

Aaron J. Oakley<sup>‡§¶</sup>, Karin V. Loscha<sup>‡¶||</sup>, Patrick M. Schaeffer<sup>‡¶</sup>, Edvards Liepinsh<sup>¶\*\*</sup>,  
Guido Pintacuda<sup>‡\*\*</sup>, Matthew C. J. Wilce<sup>§</sup>, Gottfried Otting<sup>‡</sup>, and Nicholas E. Dixon<sup>‡‡</sup>

From the <sup>‡</sup>Research School of Chemistry, Australian National University, Canberra, Australian Capital Territory 0200, Australia, the <sup>§</sup>School of Medicine and Pharmacology and School of Biomedical and Chemical Sciences, University of Western Australia, Nedlands, Western Australia 6907, Australia, and the <sup>\*\*</sup>Department of Medical Biochemistry and Biophysics, Karolinska Institutet, S-171 77 Stockholm, Sweden

During bacterial DNA replication, the DnaG primase interacts with the hexameric DnaB helicase to synthesize RNA primers for extension by DNA polymerase. In *Escherichia coli*, this occurs by transient interaction of primase with the helicase. Here we demonstrate directly by surface plasmon resonance that the C-terminal domain of primase is responsible for interaction with DnaB<sub>6</sub>. Determination of the 2.8-Å crystal structure of the C-terminal domain of primase revealed an asymmetric dimer. The monomers have an N-terminal helix bundle similar to the N-terminal domain of DnaB, followed by a long helix that connects to a C-terminal helix hairpin. The connecting helix is interrupted differently in the two monomers. Solution studies using NMR showed that an equilibrium exists between a monomeric species with an intact, extended but naked, connecting helix and a dimer in which this helix is interrupted in the same way as in one of the crystal conformers. The other conformer is not significantly populated in solution, and its presence in the crystal is due largely to crystal packing forces. It is proposed that the connecting helix contributes necessary structural flexibility in the primase-helicase complex at replication forks.

other strand is replicated as short Okazaki fragments that are later joined to generate a contiguous lagging strand (2). In prokaryotes, synthesis of both the Okazaki fragments and the nascent leading strand are initiated from primers generated by a specialist single-stranded DNA (ssDNA)<sup>1</sup>-dependent RNA polymerase called primase. The *Escherichia coli* primase is encoded by the *dnaG* gene (3), and its RNA polymerase domain is highly conserved in prokaryotic genomes (4).

In bacteria, strand separation at replication forks is carried out by the hexameric DnaB helicase (DnaB<sub>6</sub>), which uses the energy of ATP hydrolysis to translocate along the lagging strand in the 5'–3' direction (5). Electron microscopy revealed that DnaB<sub>6</sub> is a ring-shaped molecule (6) that can exist in different quaternary states with either C<sub>3</sub> (trimer of dimers) or C<sub>6</sub> symmetry, depending on conditions (7, 8). The DNA strand on which it translocates passes through its central channel, whereas the other is excluded (9, 10). It is generally thought that each subunit of DnaB is composed of two domains connected by a hinge region (11). Although there is no high resolution structure reported for the intact hexameric DnaB, the structure of its smaller N-terminal domain has been determined both by NMR spectroscopy (12) and x-ray crystallography (13). These structures were recently used in conjunction with the known crystal structure of the helicase domain of the related hexameric bacteriophage T7 gp4 helicase-primase (14) to model structures into electron density maps of DnaB<sub>6</sub> produced by image reconstruction from negative stain electron microscopy data (15). It is generally accepted that the C-terminal face of DnaB<sub>6</sub> is directed into the replication fork and contains the site of strand separation, whereas the N-terminal face points away from the fork where it would be appropriately placed to interact with the DnaG primase (16, 17).

Priming of Okazaki fragment synthesis on the lagging strand requires helicase-primase interaction. Although *E. coli* primase appears to be repeatedly recruited to the lagging strand by transient interaction with the helicase (18), the interaction between the *Bacillus stearothermophilus* homologs is sufficiently stable that a complex of the helicase with two or three molecules of primase can be isolated (19, 20).

Primase is composed of an N-terminal zinc-binding domain that mediates interaction with the ssDNA template (21, 22), a larger central domain responsible for primer synthesis (4), and

All organisms replicate DNA in a semidiscontinuous fashion (1). At each replication fork, one of the parental strands is the template for synthesis of an uninterrupted leading strand. The

\* This work was supported by research grants from the Australian Research Council, an Australian Postdoctoral Fellowship (to A. J. O.) and a Federation Fellowship (to G. O.). Data collection at the Advanced Photon Source, Chicago, was supported by the United States Department of Energy, Basic Energy Sciences, Office of Science, under contract W-31-109-Eng-38. Use of the BioCARS Sector 14 was supported by the National Institutes of Health, National Center for Research Resources, under Grant RR07707. The costs of publication of this article were defrayed in part by the payment of page charges. This article must therefore be hereby marked "advertisement" in accordance with 18 U.S.C. Section 1734 solely to indicate this fact.

The atomic coordinates and structure factors (code 1T3W) have been deposited in the Protein Data Bank, Research Collaboratory for Structural Bioinformatics, Rutgers University, New Brunswick, NJ (<http://www.rcsb.org/>).

The NMR chemical shifts of amide protons (code 6284) have been deposited in the BioMagResBank, University of Wisconsin, Madison WI (<http://www.bmrb.wisc.edu>).

<sup>§</sup> The on-line version of this article (available at <http://www.jbc.org>) contains Supplemental Data, including an additional figure.

<sup>¶</sup> These authors contributed equally to this work.

<sup>||</sup> Supported by a scholarship from the Deutscher Akademischer Austauschdienst.

<sup>‡‡</sup> To whom correspondence should be addressed. Tel.: 61-2-61254391; Fax: 61-2-61250750; E-mail: [dixon@rsc.anu.edu.au](mailto:dixon@rsc.anu.edu.au).

<sup>1</sup> The abbreviations used are: ssDNA, single-stranded DNA; AMP-PNP, adenosine-5'-( $\beta,\gamma$ -imido)triphosphate; DnaG-C, the C-terminal domain (residues 434–581) of *E. coli* DnaG primase; HSQC, heteronuclear single quantum coherence; NOE, nuclear Overhauser effect; NOESY, two-dimensional NOE spectroscopy; SPR, surface plasmon resonance (BIAcore); TOCSY, total correlation spectroscopy; RU, response unit(s); MES, 2-morpholinoethanesulfonic acid.

a C-terminal domain (residues 434–581) that interacts with DnaB<sub>6</sub> (23, 24). Although high resolution structures of the zinc-binding domain of *B. stearotherophilus* primase (25) and the central catalytic core domain of the *E. coli* enzyme (16, 26) have been published, the structure of the C-terminal domain (also termed p16, and here designated DnaG-C) has not previously been reported.

Studies of the structure and function of the DnaG-C domain have been restricted due to difficulty in expressing it in *E. coli*, presumably because it binds (and thus inactivates) DnaB in competition with the full-length primase (18, 23). Mutations in the extreme C-terminal 16 residues of primase led to defects in its function in DnaB-dependent *in vitro* replication reactions, suggesting that this region, at least, makes contacts with the helicase (23, 27). Whereas previous studies showed that a glutathione *S*-transferase-DnaG-C fusion protein is capable alone of interacting with DnaB<sub>6</sub> (24), there has been no physical demonstration that this interaction is mediated solely by the C-terminal domain of primase.

Here we report thermodynamic parameters and stoichiometry, determined by surface plasmon resonance (SPR) measurements, for the association of DnaG-C with DnaB<sub>6</sub>. The data demonstrate that the C-terminal domain is largely, if not completely, responsible for primase-helicase interactions and that up to three DnaG-C molecules are able to bind noncooperatively to the helicase hexamer. The crystal structure of DnaG-C, determined at 2.8-Å resolution, shows that the protein is an elongated molecule composed of two globular subdomains connected by a long helix. It exists in the crystalline state as an asymmetric dimer of subunits with two different conformations resulting from bending of the connecting helix at different positions, indicating that this helix is rather flexible. NMR spectroscopy was used to demonstrate in solution that a monomer-dimer equilibrium exists at high concentrations, that the connecting helix persists and appears to be straight in the monomer, and that one of the crystal conformers is most highly populated in the dimer. Thus, the other crystal conformer appears to be trapped in the solid state by crystal packing forces.

#### EXPERIMENTAL PROCEDURES

**Protein Purification**—Overproduction of DnaG, DnaG-(1–433), and DnaG-C was achieved in *E. coli* strains containing plasmid derivatives of vector pCE30, pMA200U (28), or pND706 (29), respectively, with appropriately constructed genes under control of thermoinducible tandem bacteriophage  $\lambda$  *p<sub>R</sub>* and *p<sub>L</sub>* promoters. Construction of pPL195 (*dnaG*<sup>+</sup>) (21) and pKL1176 (*dnaG-C*<sup>+</sup>) (30) have been described. To prepare plasmid pCP806 (*dnaG*-(1–433)<sup>+</sup>), the *dnaG* gene from pPL195 was transferred to the phagemid vector pMA200U, and the single-stranded form was used as template for oligonucleotide-directed mutagenesis (31) to replace codon 434 of *dnaG* with a TAA stop codon followed by an EcoRI site. Deletion of an EcoRI fragment downstream of the coding region in pCP806 yielded pCP807, which was used for overproduction of DnaG-(1–433) (see Supplemental Data for details).

Unlabeled, uniformly <sup>13</sup>C,<sup>15</sup>N-labeled, and selenomethionine-substituted DnaG-C were purified as described (30). To avoid the possibility of heterogeneity at the C terminus of the protein, DnaG primase was expressed in a suppressor-free host strain (*cf.* Ref. 30). Details of procedures for purification of primase and DnaG-(1–433), along with verification of their purity by SDS-PAGE, are given in detail in the Supplemental Data. Concentrations of primase, DnaG-(1–433), and DnaG-C were determined spectrophotometrically at 280 nm, using calculated values of  $\epsilon_{280}$  of 43,240, 30,580, and 12,660 M<sup>-1</sup> cm<sup>-1</sup>, respectively (32).

DnaB<sub>6</sub> was purified using strain AN1459/pPS562 (6). Plasmid pPS562 contains a synthetic *dnaCB* operon under transcriptional control of the tandem  $\lambda$  *p<sub>R</sub>* and *p<sub>L</sub>* promoters and directs high level overproduction of equimolar amounts of DnaB and DnaC proteins. Concentrations of DnaB<sub>6</sub> were determined by the method of Bradford (33), using bovine serum albumin as standard.

**SPR Measurements**—A Biacore 2000 instrument (Biacore AB, Uppsala, Sweden) was used to study the interactions of DnaB with DnaG as

TABLE I  
MAD phasing statistics (resolution range 50 to 2.8 Å)

	Wavelength (Å)	Phasing power <sup>a</sup>	<i>R</i> <sub>cutlis</sub> <sup>b</sup>
$\lambda$ 1 (peak)	0.979862	2.3082	0.6098
$\lambda$ 2 (inflexion)	0.980004	2.3815	0.5849
$\lambda$ 3 (remote)	0.9776	0.5733	0.9315

$$^a \langle |F_H|^2 \rangle^{1/2} / \langle |F_{PH}|^2 \rangle^{1/2} - |F_P + F_H|^2 / 2$$

$$^b \langle |F_{PH}|^2 \rangle^{1/2} / \langle |F_P + F_H|^2 \rangle^{1/2} - \langle |F_P|^2 \rangle^{1/2}$$

well as its N- and C-terminal domains. All studies were carried out at 20 °C at a flow rate of 5  $\mu$ l/min. For immobilization onto a CM5 sensor chip (Biacore), proteins were diluted into 10 mM MES (pH 6.0) (for wild-type DnaG) or a mixture of 2 volumes of 10 mM MES (pH 6.0) with 3 volumes of 10 mM HEPES (pH 7.4) (for DnaG-(1–433)). All flow cells were activated with a 7-min injection of a freshly prepared aqueous solution of 50 mM *N*-hydroxysuccinimide and 200 mM 1-ethyl-3-(3-dimethylaminopropyl) carbodiimide. DnaG was immobilized onto two flow cells to yield increases in response units (RU) of 742 and 1472. DnaG-(1–433) (1220 RU) was immobilized on a third flow cell, and one flow cell served as a control surface (CM5 chip I). All flow cells were then deactivated with 1 M ethanolamine (pH 8.5). The surface of a second CM5 sensor chip (CM5 chip II) was treated similarly to immobilize wild-type DnaG at a low level (380 RU). Wild-type DnaB<sub>6</sub> in 10 mM HEPES (pH 7.4), 10 mM MgCl<sub>2</sub>, 150 mM NaCl, 1 mM dithiothreitol, and 0.005% surfactant P20 (BIAcore buffer) at concentrations between 0.21 and 2.11  $\mu$ M (as subunits) was made to flow during 2 min over the immobilized DnaG on CM5 chip II. Elution was allowed to proceed in the same buffer for 10 min. The flow cells were regenerated by injections (2 min) of 10 mM HEPES (pH 7.4).

The streptavidin-coated sensor chip (SA chip; Biacore) was activated with three sequential injections of 1 M NaCl, 50 mM NaOH (1 min each). A solution (2 nM) of a 3'-biotinylated oligonucleotide comprising 35 thymidine residues (3'-Bio-(dT)<sub>35</sub>) in BIAcore buffer was used to yield an increase of 61 RU (6 min) on one flow cell. Another flow cell was unmodified and served as a control. DnaB<sub>6</sub> was diluted in BIAcore buffer containing 0.1 mM AMP-PNP to 2.11  $\mu$ M, and 1000 RU were immobilized (10 min) onto 3'-Bio-(dT)<sub>35</sub>. After allowing DnaB to stabilize on 3'-Bio-(dT)<sub>35</sub> for a further 9.5 min, DnaG was injected over the flow cells during 1 min. After 5 min of dissociation, the flow cells were regenerated by injection of 1 M NaCl, 50 mM NaOH (1 min). This removed DnaB<sub>6</sub>, which was then reloaded onto the chip for a new cycle. Solutions of increasing concentrations of DnaG primase were tested in this way.

The same flow cell was used to investigate the interaction of DnaG-C with ssDNA-bound DnaB<sub>6</sub>. The binding signal was increased by raising the level of immobilized 3'-Bio-(dT)<sub>35</sub> to 133 RU. The interaction was monitored as described above, except that 1900 RU of DnaB<sub>6</sub> (8.4 min) were immobilized onto the chip, and DnaG-C was injected at various concentrations.

The equilibrium dissociation constants (*K<sub>D</sub>*) of all complexes were derived from raw data by use of the BIAevaluation software (version 3.2; Biacore). Steady-state data were used to calculate the *K<sub>D</sub>* of a complex. Before fitting, binding data were corrected by subtraction of the control response due to simple refractive index change. The RU values of DnaB<sub>6</sub> bound onto the 3'-Bio-(dT)<sub>35</sub> derivatized SA surface were normalized to 1000 RU for DnaG binding or 1900 RU for DnaG-C. The curve of equilibrium response *versus* [analyte] was fitted to a 1:1 Langmuir binding model. The experimental errors in determined parameters are S.E. values calculated by BIAevaluation.

**Crystal Structure Determination**—Crystals of selenomethionine-substituted DnaG-C were grown by vapor diffusion in hanging drops (2  $\mu$ l) as described (30). Protein solutions (~4 mg/ml), initially in 0.05 M sodium acetate buffer (pH 4.6) with 2.5% polyethylene glycol 4000 and 0.1 M ammonium sulfate, were equilibrated at 4 °C over reservoirs containing the same components at twice these concentrations. X-ray data sets were collected at three wavelengths suitable for phasing based on selenium anomalous dispersion as described previously (30). Statistics for anomalous scattering in these data are given in Table I. Since the native protein crystals did not yield useful diffraction, one of the MAD data sets ( $\lambda$ 1, 2.8-Å resolution) was used as the reference data set for structure refinement. Initial phase and solvent flattening calculations were conducted in CNS (34). Arp/wARP (35) was used for further phase improvement. All model building was performed manually in O (36), with model refinement performed by REFMAC (37). Maximum

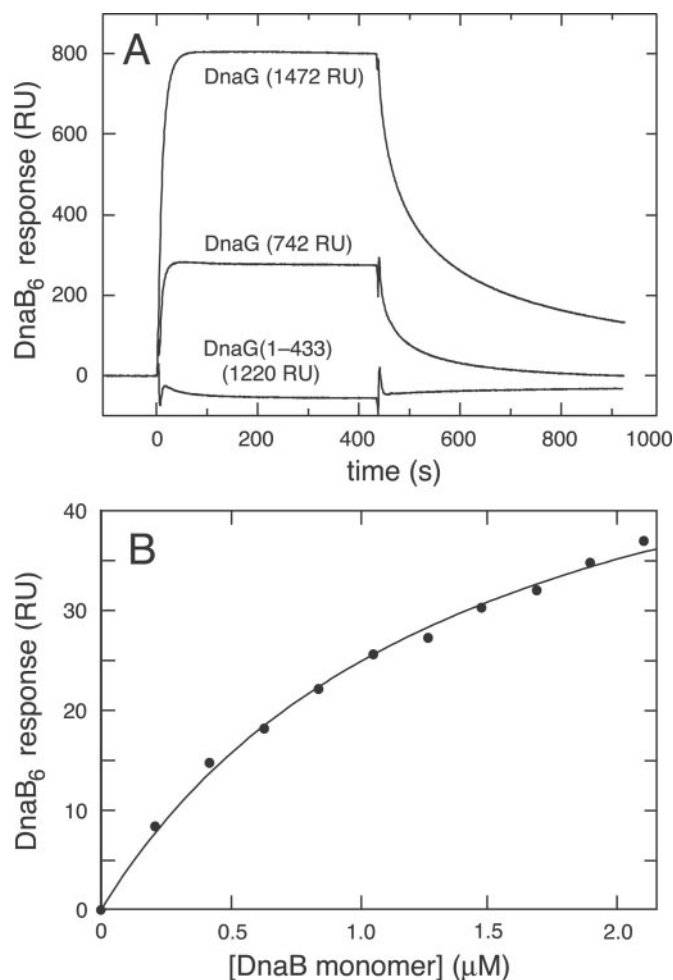


FIG. 1. Comparison of BIAcore data for the interaction of DnaB<sub>6</sub> helicase with immobilized DnaG and DnaG-(1-433). A, DnaB<sub>6</sub> (2.11 μM, as subunits) was injected over CM5 chip I (see “Experimental Procedures”). The flow cells were derivatized with 1472 and 742 RU of DnaG and 1220 RU of DnaG-(1-433). DnaG-(1-433) does not interact with DnaB. B, steady-state data for the interaction of DnaB<sub>6</sub> with immobilized DnaG (380 RU) on CM5 chip II. Equilibrium RU<sub>eq</sub> values are plotted versus [DnaB monomer]. The fit for a 1:1 binding model is shown as a solid line, calculated using  $K_D = 1.4 \mu\text{M}$ ,  $R_{\text{max}} = 60 \text{ RU}$ .

likelihood-weighted phases from REFMAC were used for  $2mF_o - dF_c$  and  $mF_o - dF_c$  electron density map calculations. Structure similarity searches were performed using the SSM server (38).

**NMR Measurements**—A 0.60 mM solution of uniformly  $^{15}\text{N}/^{13}\text{C}$ -labeled DnaG-C in 10 mM sodium phosphate (pH 6.07), 0.1 M NaCl, 1 mM dithiothreitol, 0.1% (w/v)  $\text{NaN}_3$  in 90%  $\text{H}_2\text{O}$ , 10%  $\text{D}_2\text{O}$  (30) was used for NMR experiments. Spectra were recorded at 25 °C using a Bruker DMX-600 NMR spectrometer equipped with a triple resonance cryoprobe operating at a  $^1\text{H}$  NMR frequency of 600 MHz. The backbone resonance assignments were obtained from three-dimensional HNCA, HNCO, (HCA)CONH, CBCA(CO)NH, HNCACB, HN(CA)HA, TOCSY- $^{15}\text{N}$ -HSQC, and NOESY- $^{15}\text{N}$ -HSQC spectra.  $^1\text{H}$ - $^{15}\text{N}$ -NOE data were recorded on a Varian Inova 600 NMR spectrometer.

## RESULTS

**SPR Analysis of DnaB<sub>6</sub> Binding to Immobilized DnaG and DnaG-(1-433)**—The interactions of DnaB<sub>6</sub> with immobilized full-length DnaG (65,572 Da) and a truncated form lacking the C-terminal domain (DnaG-(1-433), 48889 Da; also termed p49) were first analyzed by SPR (BIAcore). DnaB<sub>6</sub> was observed to bind only to surfaces with immobilized DnaG; no response was observed with DnaG-(1-433) even at the highest concentration (2.11 μM, as monomer) of DnaB (Fig. 1A). An equilibrium binding isotherm for the interaction of DnaB<sub>6</sub> with immobilized

DnaG was obtained using a second sensor chip with a lesser loading of DnaG (Fig. 1B). It gave a good fit to a Langmuir binding model for a 1:1 interaction, with a dissociation constant  $K_D$  of the DnaB<sub>6</sub>-DnaG complex of  $1.4 \pm 0.1 \mu\text{M}$  (with [DnaB] expressed as concentration of subunits, assuming there are six potential binding sites in the hexamer). The maximum response ( $R_{\text{max}}$ ) for DnaB<sub>6</sub> binding to this surface indicated that only about 3% of the immobilized DnaG molecules were capable of binding DnaB hexamers. Similarly inefficient and weak binding has been reported previously in a similar experiment (39). The association and dissociation phases were fast, and a large mass transport effect due to the large size of DnaB<sub>6</sub> (314 kDa) was expected. Because most of the immobilized primase was inactive, presumably because the DnaB<sub>6</sub>-binding site was occluded during covalent immobilization, it was not possible to determine the stoichiometry of the complex with this surface. Nevertheless, the interaction appeared to be a specific one, since the addition of 3 μM primase as competitor with 0.21 μM DnaB<sub>6</sub> as analyte reduced the SPR response by ~50%. Moreover, the interaction was observed to be absolutely dependent on the presence of  $\text{Mg}^{2+}$ . Since hexamerization of DnaB at the concentrations used here is dependent on  $\text{Mg}^{2+}$  (40), this also suggests that only the hexamer is capable of binding primase.

**Binding of DnaG and DnaG-C to 3'-Bio-(dT)<sub>35</sub>-immobilized DnaB<sub>6</sub>**—The influence of interaction of DnaB<sub>6</sub> with ssDNA on its association with primase has not previously been examined directly. For this purpose, we used a 3'-biotinylated oligonucleotide (3'-Bio-(dT)<sub>35</sub>) long enough that it should bind well within the central channel of the helicase but not projecting so far that it could simultaneously interact with DnaB<sub>6</sub>-bound primase. The helicase was thus immobilized via its interaction with 3'-Bio-(dT)<sub>35</sub> that had previously been bound to the streptavidin-coated surface of a Biacore SA chip. DnaB<sub>6</sub> uses the energy of ATP hydrolysis to move in the 5'-3' direction on ssDNA. It was found to bind quite stably onto immobilized 3'-Bio-(dT)<sub>35</sub> in the presence of  $\text{Mg}^{2+}$  and the nonhydrolyzable ATP analog, AMP-PNP (Fig. 2, A and B). After the DnaB surfaces had been prepared, analyte solutions containing a range of concentrations of DnaG, DnaG-C, or DnaG-(1-433) were made to flow over them until equilibrium had been reached.

Although no binding of DnaG-(1-433) was observed even at a concentration as high as 3.7 μM, both DnaG and DnaG-C were found to interact with ssDNA-bound DnaB<sub>6</sub> in a concentration-dependent manner (Fig. 2). No major artifacts like mass transfer limitations were noted, probably because the sizes of the analytes were relatively small. Although some surface degradation occurred due to slow release of DnaB<sub>6</sub>, it was negligible in the time frame of the experiments. The binding and dissociation phases for both proteins were complete in <10 s (Fig. 2, A and B), confirming the transience of the DnaB<sub>6</sub>-DnaG interaction (18) but rendering it impossible to determine accurate kinetic parameters.

The equilibrium binding isotherm for binding of DnaG-C (Fig. 2C) fit well to a 1:1 binding model, with  $K_D = 4.9 \pm 0.3 \mu\text{M}$  and  $R_{\text{max}}$  that corresponded to binding of  $3.14 \pm 0.08$  molecules of DnaG-C per hexamer of DnaB at saturation. There was no evidence of cooperativity among the three sites. The data for DnaG were limited by the accessible range of concentrations, and there was evidence of some nonspecific interaction of primase with the chip surface (Fig. 2A). Nevertheless, the binding isotherm still fit reasonably to a 1:1 Langmuir model with  $K_D = 2.8 \pm 0.4 \mu\text{M}$  (Fig. 2C).

**Crystal Structure of DnaG-C**—Previously, we reported crystallization of selenomethionine-substituted DnaG-C and data collection at a synchrotron source (30). The structure was

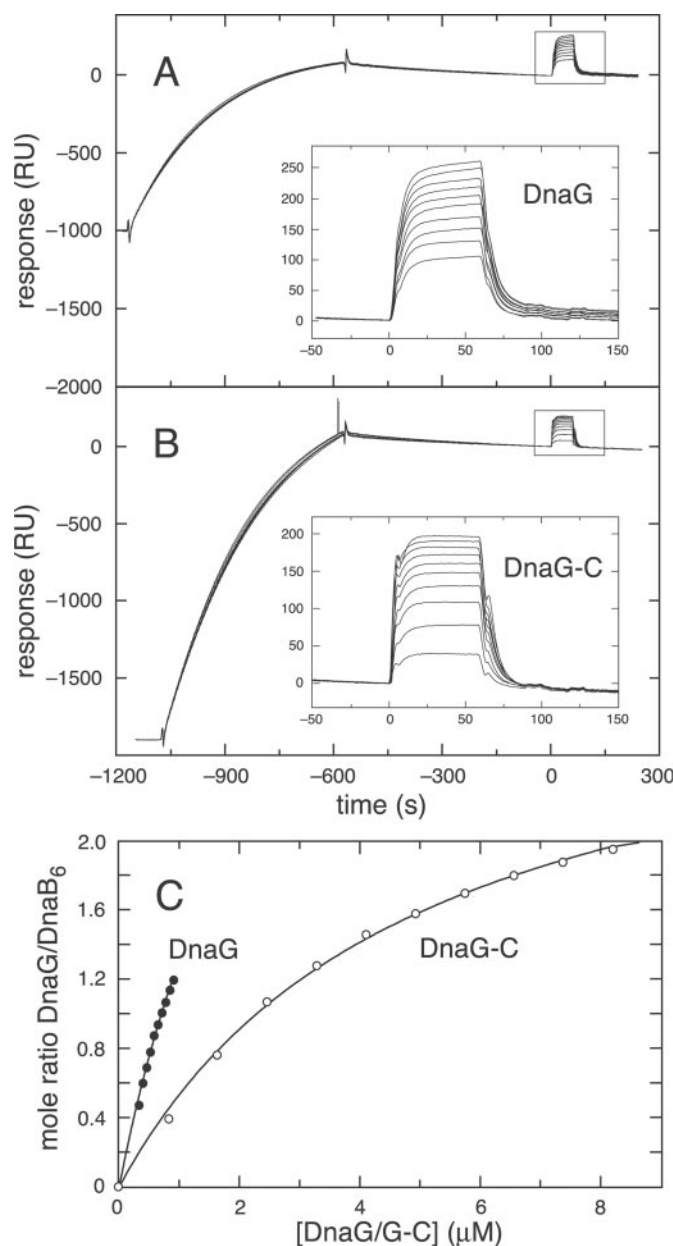


**FIG. 2. BIAcore data for the interaction of DnaG and DnaG-C with DnaB<sub>6</sub> immobilized via 3'Bio-(dT)<sub>35</sub> on a Biacore SA chip.** DnaB was immobilized onto a 3'Bio-(dT)<sub>35</sub> derivatized SA chip surface, and DnaG (A) or DnaG-C (B) was injected 9.5 min later (see "Experimental Procedures"). The curves shown in inset A are at [DnaG] from 0.32 to 0.90 μM, and curves in B are with [DnaG-C] from 0.82 to 8.20 μM. C, binding isotherms for the interaction of DnaG and DnaG-C with immobilized DnaB<sub>6</sub>. Mole ratios of bound DnaG or DnaG-C to immobilized DnaB<sub>6</sub>,  $n = ((R_{eq} \text{ of DnaG/G-C}) * (M_r \text{ of DnaB}_6)) / (M_r \text{ of DnaG} * (R \text{ of DnaB}_6))$ . The solid curves were calculated for a 1:1 binding model, with values of  $K_D = 2.8 \mu\text{M}$ ,  $n_{max} = 4.97$  (for DnaG),  $K_D = 4.9 \mu\text{M}$ ,  $n_{max} = 3.14$  (for DnaG-C).

solved at 2.8-Å resolution using phases derived from MAD data sets. Four selenium sites in the asymmetric unit were identified by Patterson search methods, using CNS (34). After refinement of their initial positions, the overall figure of merit was 0.57. This was improved to 0.75 by solvent flattening density modification. The map resulting from these phase data revealed electron density of a mainly helical protein. Interpretation of the electron density maps indicated that the four selenium sites corresponded to two buried selenomethionine residues in each of two DnaG-C monomers. A model consisting of 207 residues was built into these maps. The  $R_{cryst}$  ( $R_{free}$ ) of

**TABLE II**  
Statistics of the final X-ray structure of DnaG-C

Parameters	Values
$R_{cryst}$ (%) <sup>a</sup>	28.0 (32.6) <sup>b</sup>
$R_{free}$ (%) <sup>a</sup>	31.6 (38.7) <sup>b</sup>
Root mean square deviations from ideal geometry	
Bond lengths (Å)	0.012
Bond angles (degrees)	1.498
Torsion angles (degrees)	5.374
Chiral volumes (Å <sup>3</sup> )	0.109
Planar groups (Å)	0.004
Ramachandran plot statistics	
Residues in favorable regions (%)	88.0
Residues in allowed regions (%)	98.4

<sup>a</sup>  $r = \sum_{hkl} |F_o(hkl) - F_c(hkl)| / \sum_{hkl} |F_o(hkl)|$ .

<sup>b</sup> Figures in parentheses correspond to the highest resolution bin (2.87 to 2.80 Å).

this model reduced from 49.9 (48.7%) to 38.3 (42.7%) after 10 cycles of refinement. This reduced to 27.5 (33.0%) after another cycle of manual model building and refinement. After three more cycles of model building and refinement, the final model had  $R_{cryst} = 26.8\%$ ,  $R_{free} = 30.8\%$ . Statistics for this model are given in Table II.

Despite the limited resolution of the x-ray data, the electron density maps were readily interpretable (Fig. 3). The final model contains two DnaG-C monomers (I and II) in close interaction with each other, forming an asymmetric dimer (Fig. 4B). The N-terminal 14 residues were not visible in electron density for either monomer and were not included in the model; this is consistent with the flexibility of these residues demonstrated previously by NMR (30). The C-terminal lysine residue in monomer II was also invisible. The solvent content of the crystals was 82%, corresponding to a Matthews' coefficient of 7.22 Å<sup>3</sup>/Da.

Each monomer consists of an N-terminal bundle of  $\alpha$ - and  $3_{10}$ -helices ( $\alpha 1$ ,  $3_{10}2$ ,  $\alpha 3$ , and  $\alpha 4$ ; Fig. 4), followed by long central ( $\alpha 5$ ) and C-terminal helices ( $\alpha 6$ ) that together form a helical hairpin. Although the helical bundle is similar in both monomers, the long helix  $\alpha 5$  is kinked in a different place in each of them (Fig. 4, A and C). This could be explained by relative flexibility of helix  $\alpha 5$  and its consequent susceptibility to perturbation by the local crystal-packing environment.

Remarkably, the helical bundle is structurally similar to the N-terminal domain of the DnaB helicase (13), despite the sequence identity being only 16% (Fig. 5). These structurally conserved domains could therefore have descended from a common ancestor of mixed function. Although each DnaG-C monomer is missing the C-terminal helix ( $\alpha 7$ ) of DnaB-N, it is replaced by helix  $\alpha 5$  of the other monomer in the DnaG-C dimer. Both DnaB-N and DnaG-C exist as dimers in the crystalline state, and NMR studies (see below and Ref. 12) show that they both form (symmetric) dimers in solution at high concentrations. Nevertheless, the dimerization interfaces involve different regions of the molecular surfaces. For DnaG-C, the extended helix  $\alpha 5$  of one monomer interacts with helices  $\alpha 1$  and  $3_{10}2$  and the loop following  $3_{10}2$  in the other. In DnaB-N, dimerization occurs via an interface involving residues from helices  $\alpha 4$  and  $\alpha 6$  (12, 13). Although the dimerization interface of DnaG-C is extensive, it may have no biological significance. Earlier studies showed that both DnaG (21) and DnaG-C (30) are monomers in solution at low concentrations as would occur intracellularly, and the 3:6 stoichiometry of the DnaG-DnaB interaction makes it difficult to conceive a biochemical role for dimerization of full-length DnaG during its interaction with DnaB<sub>6</sub> or during primer synthesis.

**Solution Conformation of the DnaG-C Monomer**—The observation of two different conformations of DnaG-C in the crystal

FIG. 3. Stereodiagram of a  $2mF_o - dF_c$  electron density map of DnaG-C. Phases were calculated from the final model, shown in *stick form*. The map is contoured at  $1\sigma$ .

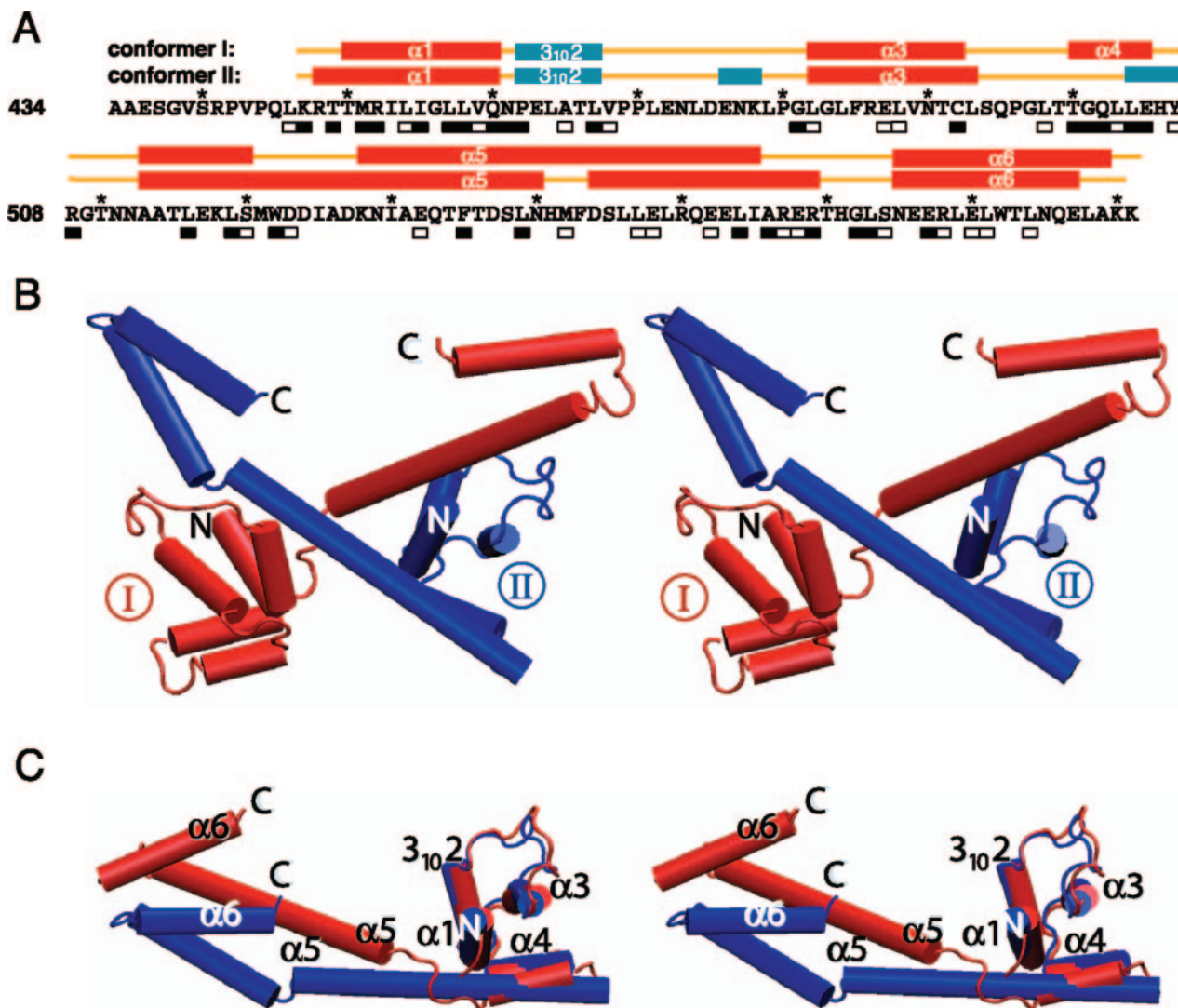
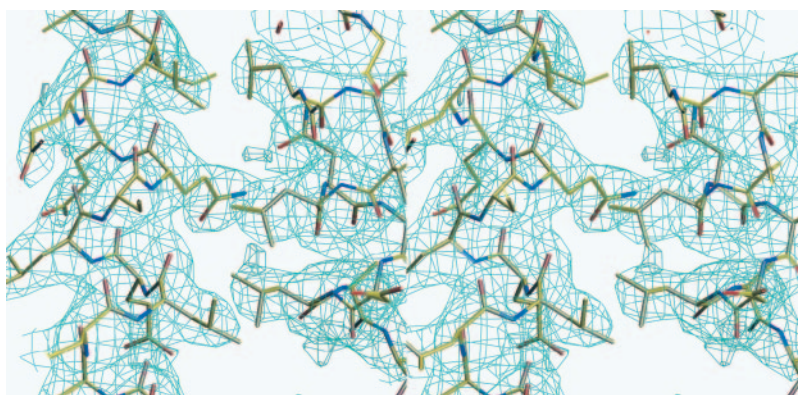


FIG. 4. Crystal structure of the DnaG-C dimer. **A**, helical regions in the two monomers I and II;  $\alpha$ - and  $3_{10}$ -helices are identified by *red* and *cyan bars*, respectively, and every 10th residue is marked by an *asterisk*. The *solid boxes* under the sequence represent residues conserved among primases from 12 bacterial species, and *open boxes* denote conservation of residue type (30). **B**, stereo view of a schematic representation of the dimer, displaying the conformers I and II in *red* and *blue*, respectively. Their N and C termini are identified. **C**, stereodiagram showing the structures of the two monomers, with the N-terminal helix bundles superimposed. The secondary structure elements and termini are labeled. The figure was drawn using VMD (53).

at pH 4.6 (Fig. 4C) raised questions about its structure in solution at higher pH and, in particular, about the existence in the monomeric state of the long naked helix ( $\alpha_5$ ) between the N-terminal globular subdomain and the C-terminal helix hairpin. This helix is reminiscent of that connecting the two globular domains of ribosomal protein L9 (41) and of calmodulin;

the latter shows a variety of conformations in the crystalline state and in solution (summarized in Ref. 42). Consequently, structural studies of DnaG-C were carried out in aqueous solution (at pH 6.1) by NMR spectroscopy, which also allowed assessment by solution data of the minor structural variability observed for the globular subdomain and the helical hairpin.

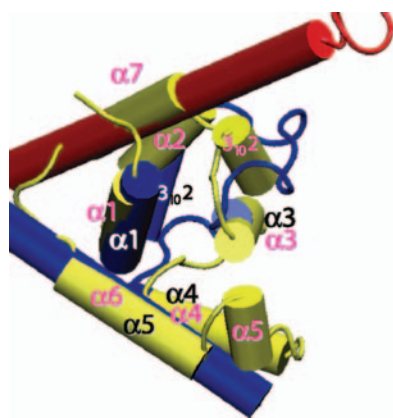


FIG. 5. The structure of DnaG-C resembles that of the N-terminal domain of DnaB. Monomers I (red) and II (blue) of DnaG-C are superimposed on DnaB-N (yellow). Elements of secondary structure are shown in black and white (DnaG) and magenta (DnaB). Comparison of the crystal structures give average root mean square deviations of 1.87 Å (over 48 C $\alpha$  atom positions) and 1.57 Å (51 C $\alpha$  atoms) for DnaG-C monomers I and II, respectively. The figure was drawn using VMD (53).

The resonances of all backbone and side chain amide protons could be observed and assigned (Fig. 6).  $^1\text{H}\{^{15}\text{N}\}$ NOEs indicated increased mobility on a subnanosecond time scale for the 16 N-terminal and three C-terminal residues of DnaG-C, in agreement with the absence of electron density for the first 14 residues in both crystal conformers and for the C-terminal residue in conformer II. All other residues showed uniformly similar  $^1\text{H}\{^{15}\text{N}\}$ NOE values within the uncertainty of the experiment. In particular, there was no evidence for increased mobility of the long connecting helix  $\alpha 5$  (data not shown).

Since helix  $\alpha 5$  is interrupted by nonhelical segments at different locations in the two crystal conformers (Fig. 4), it could plausibly form a single long helix in solution, spanning residues 513–558. As expected for an  $\alpha$ -helix, NOEs between the amide protons of sequentially neighboring residues,  $d_{\text{NN}}$ , were indeed observed for all nonoverlapping residues of this peptide segment in a three-dimensional NOESY- $^{15}\text{N}$ -HSQC spectrum. For Trp-522, Ala-526, and Asp-527, however, the sequential NOEs between the  $\alpha$ -protons and the amide protons of the following residues,  $d_{\alpha\text{N}}$ , were much more intense than the corresponding  $d_{\text{NN}}$  connectivities. This indicates that these residues predominantly sample more extended conformations than expected for an  $\alpha$ -helix, in agreement with the bend observed in this segment in conformer I. In contrast, the kink near Met-542 in conformer II was not supported by a strong  $d_{\alpha\text{N}}$  NOE, and an extensive set of  $d_{\alpha\text{N}}(i, i + 3)$  NOEs observed for the segment between Asn-529 and Glu-558 indicated  $\alpha$ -helical conformation. This identifies this kink as a crystallization artifact. In solution, the  $\alpha$ -helix thus appears to be regular except for the segment between residues 522 and 527, as observed for crystal conformer I.

**DnaG-C Dimerizes at High Concentrations in Solution—**Closer inspection of the three-dimensional NOESY- $^{15}\text{N}$ -HSQC and two-dimensional NOESY spectra revealed several NOEs that could only be interpreted as intermolecular NOEs in a homodimer. Sizeable NOEs were identified between the aromatic ring of Phe-535 and the methyl groups of Leu-454 and Leu-464, which were also involved in weak NOEs with the amide proton of Phe-535. Furthermore, a weak NOE was observed for the amide proton of Glu-532, which could only be explained as an interaction with a methyl group of Leu-464. These NOEs are in agreement with the dimer interface observed in the crystal structure, indicating that this interface in solution is similar to that in the crystal.

The asymmetry of the DnaG-C dimer in the crystal structure suggests a nonrigid interface, and the interaction between monomers is relatively weak. Gel filtration experiments indicated monomeric protein at lower concentrations (30), and sedimentation equilibrium experiments failed to detect a monomer-dimer equilibrium at concentrations up to 5 mg/ml (data not shown). Furthermore, studies of the concentration dependence of  $^{15}\text{N}$ -HSQC spectra (see below) suggest a dimerization constant in the low millimolar range.

**Transient Existence of Different Conformational States in Solution—**Since the NMR data yielded only a single set of resonances, the dimer in solution is either symmetric or the averaging among different conformations is rapid on the NMR time scale (ms). The observation of  $d_{\text{NN}}$  NOEs in the presence of strong  $d_{\alpha\text{N}}$  NOEs in the segment between Trp-522 and Asp-527 is difficult to explain by a single conformation but is compatible with an equilibrium between a straight helix  $\alpha 5$  and a disrupted helix as in conformer I. The crystal structure shows that burial of the side chain of Phe-535 in the hydrophobic pocket of the globular N-terminal subdomain of the other monomer of DnaG-C can be achieved simultaneously for both monomers in the dimer by bending the  $\alpha 5$  helix. Straightening of  $\alpha 5$  would, however, disrupt the intermolecular interaction of Phe-535 for at least one of the monomers. Existence of an equilibrium between a straight and a disrupted helix provides the most plausible interpretation of the NOEs observed in solution.

The transient existence of different conformational states is supported by the solvent protection of exchangeable amide protons. The three-dimensional NOESY- $^{15}\text{N}$ -HSQC spectrum displayed cross-peaks between the water and the amide protons of DnaG-C arising from amide proton exchange with the water or by exchange-relayed NOEs with hydroxyl protons of serine, threonine, or tyrosine residues. The crystal structure revealed no cavities that could enclose tightly bound water molecules, so the possibility of strong intermolecular NOEs with water can be disregarded (43). Intense exchange cross-peaks were observed for the unstructured N-terminal segment and the loop regions between the helices (Fig. 7). Relatively intense cross-peaks were also observed for some of the solvent-exposed amide protons at the amino-terminal ends of the helices. With few exceptions, however, the helices were characterized by slow amide-proton exchange rates as expected for hydrogen-bonded protons. The crystal structure showed that, in general, the side chain hydroxyl groups of serine and threonine in the  $\alpha$ -helices were close to the amide protons of the following amino acid residues, establishing a pathway for exchange-relayed NOEs. The remaining cross-peaks suggested that helix  $\alpha 4$  is less stable than helices  $\alpha 1$  and  $3_{10}2$ ; this is consistent with it being  $\alpha$ -helical in only one of the two crystal conformers (Fig. 4). The exchange cross-peaks of Asp-523 and the following residues support the presence of a structural irregularity in this part of helix  $\alpha 5$  but do not indicate as high solvent exposure as expected for the crystal conformer I. Like the NOEs discussed above, the relatively high, yet incomplete protection from solvent access observed in this region supports the existence of an equilibrium between a bent and a straight  $\alpha 5$  helix. Similarly, the absence of a significant exchange cross-peak for Phe-543 supports the NOE data, indicating that the helix bend observed in this region in conformer II is not significantly populated in solution. The cross-peak of Gln-533 overlapped with the extremely strong cross-peak of Ser-440 and thus could not be interpreted. The exchange cross-peaks observed for helix  $\alpha 5$ , however, suggested that this helix is less stable than the N-terminal helices.

Different peak intensities in the  $^{15}\text{N}$ -HSQC spectrum (Fig. 6) are indicative of different transverse relaxation times for dif-

**FIG. 6.  $^{15}\text{N}$ -HSQC NMR spectrum of uniformly  $^{15}\text{N}/^{13}\text{C}$ -labeled DnaG-C.** The spectrum was recorded at 25 °C and a  $^1\text{H}$  NMR frequency of 600 MHz, using a 0.6 mM solution of labeled DnaG-C in 90%  $\text{H}_2\text{O}/10\%$   $\text{D}_2\text{O}$  at pH 6.07. The cross-peaks of the backbone amide protons are assigned with the one-letter amino acid symbols and residue numbers as in Fig. 4. Cross-peaks with a  $^1\text{H}$  chemical shift of  $>10$  ppm are from the side chains from Trp-522 and Trp-572. Cross-peaks from side chain amides are connected by horizontal lines.

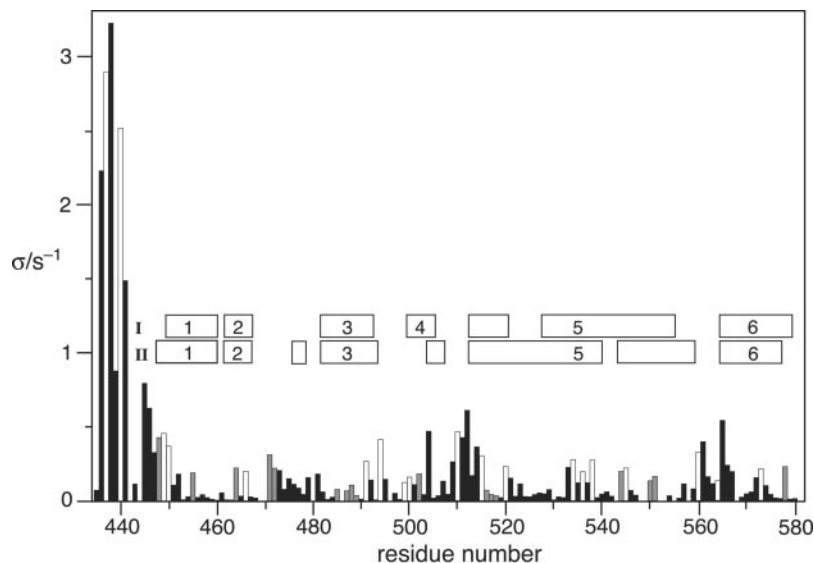
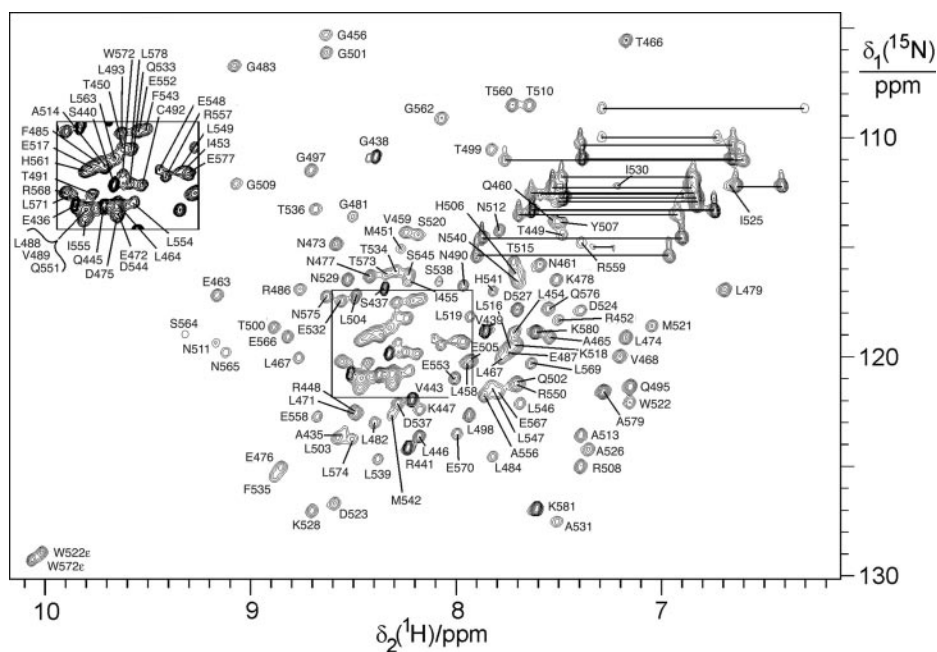


**FIG. 7. Water-protein cross-peaks versus amino acid sequence.** The horizontal boxes delineate the helices identified in the crystal structure of monomers I and II (Fig. 4). The peak heights of the cross-peaks between water and amide protons observed in the three-dimensional NOESY- $^{15}\text{N}$ -HSQC spectrum are plotted. The filled and gray bars, respectively, correspond to resolved and overlapped cross-peaks. The open bars identify serine and threonine residues. The vertical scale is an approximate measure of the magnetization transfer rates between water and protein protons due to chemical exchange, NOE, and exchange-relayed NOE. The scale was calibrated by comparing the cross-peak and diagonal peak intensities of Gly-438, using the initial rate approximation.

ferent residues. Judging the peak intensities by the number of contour lines in the  $^{15}\text{N}$ -HSQC spectrum, the weakest cross-peaks were observed for residues Met-451, Asn-511, Ile-530, Met-542, Arg-559, Ser-564, and Asn-565. The last three of these are in the loop structure of the C-terminal helix hairpin, and their resonances could be broadened by conformational exchange or attenuated by chemical exchange with water protons. Similarly, Asn-511 is located in a loop region of high solvent exposure. Most interestingly, however, Met-451, Ile-530, and Met-542 are located near the dimer interface. Their weak peak intensities suggest that the dimer interface is dynamic on a microsecond to millisecond time scale. This notion is supported by the fact that a large number of residues for which relatively weak cross-peaks were observed in the  $^{15}\text{N}$ -HSQC spectrum are located near the interface (Fig. 8).

In the situation of fast chemical exchange between monomeric and dimeric forms of the protein, one would expect that the exchange-broadened signals narrow upon dilution of the protein. This was investigated by recording  $^{15}\text{N}$ -HSQC spectra at protein concentrations of 0.4, 0.04, and 0.004 mM (data not shown). Only minor chemical shift changes were observed.

A  $>15\%$  increase in the relative peak intensities observed for Asp-524, Ala-526, Ala-531, and Phe-535 at 0.04 versus 0.4 mM supported the notion that the proportion of monomer increased upon dilution. The peak intensities did not grow further upon dilution to 0.004 mM, suggesting that insignificant amounts of dimer were left at 0.04 mM. That changes in chemical shifts were minor indicates that the monomeric species is predominant also at high concentrations, consistently with a dimerization constant of  $>1$  mM.

A  $>15\%$  increase in the relative peak intensities was also observed for residues 556, 558, 559, 561, 562, 564, and 565 at 0.04 versus 0.4 mM. These residues are located in the loop of the C-terminal helix hairpin, far from the dimerization interface. This may be explained by some nonspecific protein aggregation at the higher concentration.

**Further Evidence That Crystal Conformer I Is Most Highly Populated in Solution**—Conformers I and II also show structural differences in the globular N-terminal subdomain. For example, Asn-473 has positive and negative  $\phi$  angles in conformers I and II, respectively. A positive  $\phi$  angle is indicated in solution, since the NOEs between Asn-473  $\text{H}^{\text{N}}$  and the  $\alpha$  protons of Asn-

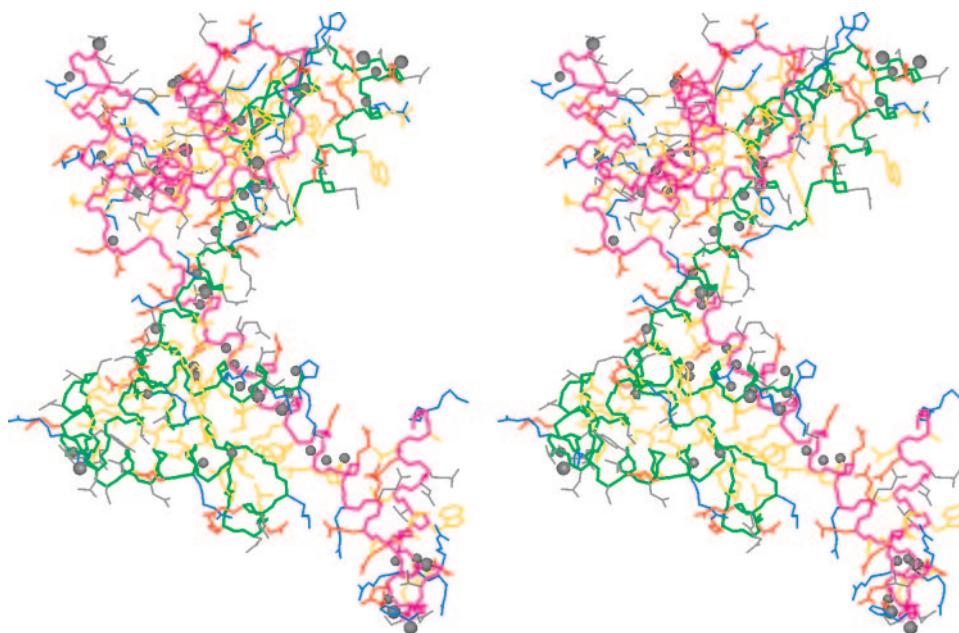


FIG. 8. Stereo view of the crystal structure of DnaG-C highlighting sites of exchange broadening identified in the  $^{15}\text{N}$ -HSQC NMR spectrum. The backbones of conformers I and II are drawn in magenta and green, respectively. The heavy atoms of the amino acid side chains are drawn in the colors: yellow for hydrophobic (Ala, Cys, Ile, Leu, Met, Phe, Pro, Trp, and Val), gray for uncharged hydrophilic (Asn, Gln, Ser, Thr, and Tyr), red for negatively charged (Asp and Glu), and blue for positively charged (Arg, His, and Lys) residues. Gray spheres identify backbone amide protons for which broadened cross-peaks were observed in the  $^{15}\text{N}$ -HSQC spectrum. Large and small spheres correspond to two and three contour levels, respectively, observed in Fig. 6. The figure was drawn using MOLMOL (54).

473 and Glu-472 were much stronger than the NOE with Glu-472  $\text{H}^{\text{N}}$ . Glu-472 is involved in crystal contacts in conformer II. Second, Thr-510 assumes very different  $\psi$  angles in conformers I and II. Again, the observation of intense  $\text{H}^{\text{N}}$ - $\text{H}^{\text{N}}$  NOEs between Gly-509 and Thr-510 but not between Asn-511 and Asn-512 is in agreement with conformer I but opposite to expectations for conformer II. In the crystal structure, residues Asn-511 and Asn-512 in monomer II and the entire loop from His-506 to Asn-511 in monomer I are engaged in crystal contacts.

Both conformers have very similar backbone conformations in the helix hairpin at their C termini, except that the  $\phi$  angle of His-561 is negative in conformer I and positive in II, resulting in its amide proton being oriented in an almost opposite direction. The set of NOEs observed between His-561  $\text{H}^{\text{N}}$  and other backbone protons again agreed closely with conformer I but not with II. In particular, there was no strong intraresidual  $\text{H}^{\alpha}$ - $\text{H}^{\text{N}}$  NOE indicative of a positive  $\phi$  angle for His-561. This observation may be explained by the presence of extensive crystal contacts involving this residue in monomer II. In monomer I, there is only a single 3.4-Å hydrogen bond between His-561 oxygen and the symmetry-related Ser-564 nitrogen atom.

In conclusion, the NMR data show that the structure of DnaG-C in solution is similar to the x-ray conformer I, whereas the structure of conformer II seems to be distorted by crystal contacts. In particular, the subdomain structure with a globular domain at the N terminus and a helix hairpin at the C terminus of DnaG-C is confirmed, including the long helical section connecting the two subdomains. There is evidence for a dynamic monomer-dimer equilibrium in solution at the concentration used for NMR, where helix  $\alpha 5$  appears to be straight in the monomer and bent in the segment of residues Trp-522 to Asp-527 in the dimer.

#### DISCUSSION

**DnaG-C Contains All Determinants for Helicase Binding**—The similarity of the independently determined values of  $K_D$  from SPR experiments with DnaG and DnaG-C (Figs. 1 and 2) and the lack of observable interaction of DnaB<sub>6</sub> with immobi-

lized DnaG-(1–433) (Fig. 1A) indicate that all of the contacts involved in interaction of DnaG with DnaB<sub>6</sub> are localized in the C-terminal domain. The data confirm earlier suggestions (18) that primase-helicase interactions in *E. coli* are rather transient, showing fast on and off rates, and are weak, with values of  $K_D$  in the micromolar range (24, 39). It should be noted that in the replisome, full-length DnaG would be expected to bind simultaneously via its C-terminal domain to DnaB<sub>6</sub> and via its zinc-binding domain and catalytic domains to the extended ssDNA template produced by helicase action. In this context, the helicase-primase interaction might be expected to be considerably stronger. Nevertheless, the similarity of values of  $K_D$  for binding of DnaB<sub>6</sub> to covalently immobilized primase (Fig. 1B) and for interaction of primase with DnaB<sub>6</sub> that had been immobilized via its interaction with a short ssDNA indicates that interaction of DnaB<sub>6</sub> with ssDNA in its central channel (Fig. 2C) does not significantly influence its interaction with DnaG.

We found (Fig. 2C) that a maximum of three molecules of DnaG-C bind to the DnaB hexamer and that there was no evidence of strong cooperativity. This is consistent with previous results obtained with full-length DnaG from *E. coli* (44) and *B. stearothermophilus* (19, 20) and supports a model wherein DnaB<sub>6</sub> acts at some stages as a trimer of dimers ( $C_3$  symmetry). The helicase has been shown to have three sites for binding (dimers) of its loading partner, DnaC (45), and nucleotides (46). Although our data with the full-length DnaG (Fig. 2C) might suggest that DnaB<sub>6</sub> is capable of binding more than three molecules of primase, they are far less reliable because they necessarily cover a very limited portion of the binding isotherm.

**Functional Significance of DnaG-C Dimerization**—The crystal structure of DnaG-C reveals a highly elongated protein with a structure related to that of the N-terminal domain of DnaB (Fig. 5). Like DnaB-N, DnaG-C exists in the crystalline state as a dimer, although in this case at least one of the monomers is trapped by crystal packing forces in a conformation that is not significantly populated in solution (Fig. 4). NMR spectroscopy

was used to show that a dimer also exists in solution at high concentrations, where the predominant structure of the individual protein molecules resembles crystal conformer I (Fig. 4). Given that both DnaG and DnaG-C are monomers at physiological concentrations (21, 30), that there is now ample evidence that DnaB<sub>6</sub> contains an odd number of (*i.e.* three) binding sites for primase (see also Refs. 20 and 44), and that the weakness of interactions between the *E. coli* proteins should ensure that no more than one primase monomer would bind DnaB<sub>6</sub> at any one time during their interaction *in vivo* in priming Okazaki fragment synthesis, the biological significance of the existence of DnaG-C dimers is uncertain.

Nevertheless, some residues at the dimer interface have been conserved during evolution. Although the DnaG-C domain is more variable among bacterial species than is the central RNA polymerase domain (4), there are now at least 11 species in which overall sequence identity with the *E. coli* protein is >30% (30). Many of the most conserved residues (Fig. 4A) are observed in the crystal structure to pack in the hydrophobic cores of the globular subdomains, and, as might be expected, exposed regions of the connecting helix are poorly conserved. Exceptions to this are Phe-535 and Leu-539, the side chains of which pack in the dimer against a conserved hydrophobic patch on the surface of the N-terminal subdomain in the other monomer (*e.g.* Leu-454, Leu-457, and Leu-467). This suggests either that dimerization of primase is involved in some aspect of its function (other than interaction with DnaB<sub>6</sub>) or that these residues form hydrophobic surfaces for interaction with another protein. Another protein that has been shown to interact with primase is SSB, the ssDNA-binding protein. This interaction involves a single molecule of primase remaining associated with a completed primer while contacting SSB bound on the following ssDNA template (47). It seems plausible that the SSB-primase interaction might also be mediated via the DnaG-C domain, but this is apparently yet to be examined experimentally.

**Functional Significance of Flexibility of DnaG-C**—A remarkable aspect of the structure of DnaG-C is the high degree of flexibility of the central helix ( $\alpha 5$ ), which is interrupted in different places in the two crystal conformers (Fig. 4) but appears to be mostly intact in solution. Previous work with versions of primase with mutations in the C-terminal helix hairpin has shown this region (at least) to be involved in interaction with DnaB<sub>6</sub> (23, 27), and conserved surface residues (Fig. 4A) that might be important for this interaction include Arg-559 and Glu-567. If all sites of interaction with DnaB<sub>6</sub> are indeed located in this C-terminal subdomain, then the flexibility of  $\alpha 5$  could allow the remainder of DnaG to search a larger conformational space to help it locate priming sites on the single strand of DNA emerging from the central channel of DnaB<sub>6</sub>.

**Site of Interaction of DnaG-C within DnaB<sub>6</sub>**—There is currently debate concerning the site of interaction of primase in DnaB<sub>6</sub> (20). As determined originally by NMR studies of larger N-terminal fragments of *E. coli* DnaB, the folded portion of DnaB-N comprises residues 24–136 (48), and some mutations within this domain have been observed to affect the interaction between DnaB<sub>6</sub> and primase (49). However, by itself, DnaB-N-(24–136) is an unstable protein that is partly unfolded at 37 °C (50), which probably means that the structure of this part of DnaB<sub>6</sub> is very easy to destabilize by mutagenesis.

These mutational data contrast with those from two other studies that suggest involvement in primase binding of regions in the interdomain hinge (residues 136 to ~170) and the C-terminal domain of DnaB. Stordal and Maurer (51) presented data on the I135N, I141T, and L156P mutants that were consistent with the hinge being a site for interaction with DnaG, and Lu *et al.* (24) used deletion analysis to map an interaction

site to the region in the C-terminal domain between Tyr-210 and Val-255. On the other hand, *B. stearothermophilus* DnaB<sub>6</sub> forms a stable complex with both *B. stearothermophilus* DnaG and its C-terminal domain, and although neither the N- or C-terminal domains of *B. stearothermophilus* DnaB interact separately with DnaG (19), mutagenesis of conserved residues in the interdomain hinge of DnaB (corresponding to Ile-135 and Ile-141 in the *E. coli* protein) did compromise its interaction with the *B. stearothermophilus* primase (20).

Although there is evidence, therefore, for interaction of DnaG-C with the hinge in DnaB<sub>6</sub>, we were unable to detect any sign of interaction of DnaG-C with <sup>2</sup>H(70%)/<sup>13</sup>C/<sup>15</sup>N-labeled DnaB-N-(1–161) (52) by NMR spectroscopy at concentrations near 0.5 mM, where very weak interactions would have been detected (data not shown). DnaB-N-(1–161) contains 25 residues from the hinge region that are unstructured in solution (48), and it includes Ile-135, Ile-141, and Leu-156. There are two possible explanations. It could be that in intact DnaB<sub>6</sub>, but not in DnaB-N-(1–161), the hinge region is structured and recognizable by primase. A second possibility is that mutations in residues in the hinge (and also destabilizing mutations within DnaB-N) affect the capacity of the N-domain to dimerize (12, 13) and that dimerization of DnaB-N in DnaB<sub>6</sub> is required to generate the primase binding site. This would be consistent with the maximum capacity of the DnaB hexamer to bind three molecules of DnaG-C (Fig. 2) and the observation of C<sub>3</sub> symmetry in the complex of the intact *B. stearothermophilus* proteins (20).

**Acknowledgments**—We are grateful to Subhash Vasudevan and Chris Penington for construction of plasmids expressing DnaG-(1–433), Max Keniry and Bogdan Bancia for NMR relaxation studies, and Simon Bennett for electrospray ionization mass spectrometry measurements.

#### REFERENCES

- Kornberg, A., and Baker, T. A. (1992) *DNA Replication*, 2nd Ed., W. H. Freeman & Co., New York
- Ogawa, T., and Okazaki, T. (1980) *Annu. Rev. Biochem.* **49**, 421–457
- Bouché, J. P., Zechel, K., and Kornberg, A. (1975) *J. Biol. Chem.* **250**, 5995–6001
- Aravind, L., Leipe, D. D., and Koonin, E. V. (1998) *Nucleic Acids Res.* **26**, 4205–4213
- LeBowitz, J. H., and McMacken, R. (1986) *J. Biol. Chem.* **261**, 4738–4748
- San Martin, M. C., Stamford, N. P. J., Dammerova, N., Dixon, N. E., and Carazo, J. M. (1995) *J. Struct. Biol.* **114**, 167–176
- Yu, X., Jezewska, M. J., Bujalowski, W., and Egelman, E. H. (1996) *J. Mol. Biol.* **259**, 7–14
- Donate, L. E., Llorca, Ó., Bárcena, M., Brown, S. E., Dixon, N. E., and Carazo, J. M. (2000) *J. Mol. Biol.* **303**, 383–393
- Jezewska, M. J., Rajendran, S., Bujalowska, D., and Bujalowski, W. (1998) *J. Biol. Chem.* **273**, 10515–10529
- Kaplan, D. L. (2000) *J. Mol. Biol.* **301**, 285–299
- Nakayama, N., Arai, N., Kaziro, Y., and Arai, K. (1984) *J. Biol. Chem.* **259**, 88–96
- Weigelt, J., Brown, S. E., Miles, C. S., Dixon, N. E., and Otting, G. (1999) *Structure* **7**, 681–690
- Fass, D., Bogden, C. E., and Berger, J. M. (1999) *Structure* **7**, 691–698
- Sawaya, M. R., Guo, S., Tabor, S., Richardson, C. C., and Ellenberger, T. (1999) *Cell* **99**, 167–177
- Yang, S., Yu, X., VanLoock, M. S., Jezewska, M. J., Bujalowski, W., and Egelman, E. H. (2002) *J. Mol. Biol.* **321**, 839–849
- Keck, J. L., Roche, D. D., Lynch, A. S., and Berger, J. M. (2000) *Science* **287**, 2482–2486
- Frick, D. N., and Richardson, C. C. (2001) *Annu. Rev. Biochem.* **70**, 39–80
- Tougu, K., Peng, H., and Mariani, K. J. (1994) *J. Biol. Chem.* **269**, 4675–4682
- Bird, L. E., Pan, H., Soultanas, P., and Wigley, D. B. (2000) *Biochemistry* **39**, 171–182
- Thirlway, J., Turner, I. J., Gibson, C. T., Gardiner, L., Brady, K., Allen, S., Roberts, C. J., and Soultanas, P. (2004) *Nucleic Acids Res.* **31**, 2977–2986
- Stamford, N. P. J., Lilley, P. E., and Dixon, N. E. (1992) *Biochim. Biophys. Acta* **1132**, 17–25
- Kusakabe, T., and Richardson, C. C. (1996) *J. Biol. Chem.* **271**, 19563–19570
- Tougu, K., and Mariani, K. J. (1996) *J. Biol. Chem.* **271**, 21391–21397
- Lu, Y.-B., Ratnakar, P. V. A. L., Mohanty, B. K., and Bastia, D. (1996) *Proc. Natl. Acad. Sci. U. S. A.* **93**, 12902–12907
- Pan, H., and Wigley, D. B. (2000) *Structure* **8**, 231–239
- Podobnik, M., McInerney, P., O'Donnell, M., and Kuriyan, J. (2000) *J. Mol. Biol.* **300**, 353–362
- Tougu, K., and Mariani, K. J. (1996) *J. Biol. Chem.* **271**, 21398–21405
- Elvin, C. M., Thompson, P. R., Argall, M. E., Hendry, P., Stamford, N. P. J.,

- Lilley, P. E., and Dixon, N. E. (1990) *Gene (Amst.)* **87**, 123–126
29. Love, C. A., Lilley, P. E., and Dixon, N. E. (1996) *Gene (Amst.)* **176**, 49–53
30. Loscha, K., Oakley, A. J., Bancia, B., Schaeffer, P. M., Prosselkov, P., Otting, G., Wilce, M. C. J., and Dixon, N. E., (2004) *Protein Expression Purif.* **33**, 304–310
31. Kunkel, T. A., Bebenek, K., and McClary, J. (1991) *Methods Enzymol.* **204**, 125–139
32. Gill, S. C., and von Hippel, P. H. (1989) *Anal. Biochem.* **182**, 319–326
33. Bradford, M. M. (1976) *Anal. Biochem.* **72**, 248–254
34. Brünger, A. T., Adams, P. D., Clore, G. M., DeLano, W. L., Gros, P., Grosse-Kunstleve, R. W., Jiang, J. S., Kuszewski, J., Nilges, M., Pannu, N. S., Read, R. J., Rice, L. M., Simonson, T., and Warren, G. L. (1998) *Acta Crystallogr. Sect. D* **54**, 905–921
35. Perrakis, A., Sixma, T. K., Wilson, K. S., and Lamzin, V. S. (1997) *Acta Crystallogr. Sect. D* **53**, 448–455
36. Jones, T. A., Zou, J. Y., Cowan, S. W., and Kleindgaard, M. (1991) *Acta Crystallogr. Sect. A* **47**, 110–119
37. Winn, M. D., Isupov, M. N., and Murshudov, G. N. (2001) *Acta Crystallogr. Sect. D* **57**, 122–133
38. Krissinel, E., and Henrick, K. (2004) *Acta Crystallogr. Sect. D* **60**, 2256–2268
39. Yuzhakov, A., Turner, J., and O'Donnell, M. (1996) *Cell* **86**, 877–886
40. Bujalowski, W., Klonowska, M. M., and Jezewska, M. J. (1994) *J. Biol. Chem.* **269**, 31350–31358
41. Hoffman, D. W., Cameron, C. S., Davies, C., White, S. W., and Ramakrishnan, V. (1996) *J. Mol. Biol.* **264**, 1058–1071
42. Fallon, J. L., and Quioco, F. A. (2003) *Structure* **11**, 1303–1307
43. Otting, G. (1997) *Prog. NMR Spectr.* **31**, 259–285
44. Mitkova, A. V., Khopde, S. M., and Biswas, S. B. (2003) *J. Biol. Chem.* **278**, 52253–52261
45. Bárcena, M., Ruiz, T., Donate, L. E., Brown, S. E., Dixon, N. E., Radermacher, M., and Carazo, J. M. (2001) *EMBO J.* **20**, 1462–1468
46. Jezewska, M. J., and Bujalowski, W. (1996) *J. Biol. Chem.* **271**, 4261–4265
47. Yuzhakov, A., Kelman, Z., and O'Donnell, M. (1999) *Cell* **96**, 153–163
48. Miles, C. S., Weigelt, J., Stamford, N. P. J., Dammerova, N., Otting, G., and Dixon, N. E. (1997) *Biochem. Biophys. Res. Commun.* **231**, 126–130
49. Chang, P., and Mariani, K. J. (2000) *J. Biol. Chem.* **275**, 26187–26195
50. Williams, N. K., Prosselkov, P., Liepinsh, E., Line, I., Sharipo, A., Littler, D. R., Curmi, P. M. G., Otting, G., and Dixon, N. E., (2002) *J. Biol. Chem.* **277**, 7790–7798
51. Stordal, L., and Maurer, R. (1996) *J. Bacteriol.* **178**, 4620–4627
52. Weigelt, J., Miles, C. S., Dixon, N. E., and Otting, G. (1998) *J. Biomol. NMR* **11**, 233–234
53. Humphrey, W., Dalke, A., and Schulten, K. (1996) *J. Mol. Graphics* **14**, 33–38
54. Koradi, R., Billeter, M., and Wüthrich, K. (1996) *J. Mol. Graphics* **14**, 51–55